# On the Optimum Die Angle in Rod Drawing Process Considering Strain-hardening Effect of Material

**M.M. Mahdavi***
PhD Candidate

**H. Haghighat†**
Associate Professor

*In this paper, rod drawing ‡process of strain-hardening materials is investigated by analytical, numerical and experimental methods. The classic upper bound solution, based on the assumption of perfect plasticity, has been extended to consider the work-hardening of the material during the drawing process. For a given process conditions and mechanical properties of the rod material, the power terms and the required drawing force are determined and optimized with respect to the die angle. The results afforded by this solution agree with data from finite element simulation, using the finite element code DEFORM 2D, and some experiments performed by the authors. It is shown that the drawing force and the optimum die angle are affected primarily by the work-hardening exponent. The amount of drawing force increases as work-hardening of material considers in the analytical solution and by increasing the work-hardening exponent, the drawing force and the optimum die angle are decreased. It is also shown that by increasing the work-hardening exponent of the rod material, the maximum possible reduction in area is increased.*

*Keywords*: Rod drawing, Work-hardening, Optimum die angle

## 1 Introduction

Rod products cover a wide range of applications, including shafts for power transmission, machine and structural components, blanks for bolts and rivets, etc. A wide variety of rods can be obtained by means of drawing process. In rod drawing, the cross section of a round section rod is reduced by pulling it through one opening die, Figure (1). Pulling of rod through the die is done by applying of a drawing force applied to the rod at the exit side of the die. Drawing of rods from round section rods is generally accomplished as a single pass operation which means that the rod is pulled through one die opening. Because the starting rod has a large diameter, it is in the form of a straight cylindrical rod. The main variables in this forming process are the die angle, the reduction in area, the friction factor and the flow stress of rod material. The optimization of the rod drawing process has been slightly improved by the recent theoretical and numerical developments in mechanics.

---

* PhD Candidate, Mechanical Engineering Department, Razi University, Kermanshah, Iran.
†Associate Professor, Mechanical Engineering Department, Razi University, Kermanshah, Iran, hhaghighat@razi.ac.ir
Manuscript received December 6, 2018; revised February 13, 2019; accepted February 15, 2019.

Different analytical, numerical, empirical and experimental methods have been conducted for decades in order to determine the optimum die angle, which would give the minimum drawing force, in rod drawing process of materials without work-hardening, perfect plastic materials. In these studies the effects of die angle, friction and area reduction ratio on the optimum die angle have been investigated. Wistreich [2] carried out an extensive experimental program on wire drawing. Avitzur [3, 4] used the upper bound method to the wire drawing process.

One most commonly equation adopted in the industrial practice presented by Avitzur [5]. The equation allows one to compute an upper bound value for the wire drawing force, assuming perfect plasticity for the wire material. The optimum die angle calculated for different high drawing speeds, wire diameters, frictional conditions and mechanical properties of the billet material was given by Critrescru [6]. An attempt has been made by Panteghini and Genna [7] to consider the work hardening effects on optimization of wire drawing forces but their solution was relatively
simple. Chevalier [8] investigated the influence of geometric parameters and the friction condition on the quality of the final wire using finite element simulation. One of the main tools today available to study metal forming processes is the finite element method. The optimization of a real industrial process implies parametric studies that involve many different values of the parameters and using this method, several different models should be developed [8]. Zhao et al. [9, 10] carried out work on drawing die optimization and analyzed two kinematically admissible velocity fields through hyperbolic and elliptic dies. Rubio et al. [11] applied the slab method and the finite element method to calculate the drawing force necessary to carry out a wire and a plate drawing process. A comparative study between analytical models and FEM results was presented by Luis et al. [12] in order to obtain forces, energies, stresses and strains which are involved in the wire drawing process. Chen and Huang [13] used the finite element and the Taguchi methods to optimize the process parameters of the wire drawing process.

Gonzalez et al. [14] applied the slab method and the finite element method to prediction the drawing force necessary to carry out a rod drawing process. As opposed to the classical slab method, the equations account for internal material distortion. It incorporated the shear force in the von Misses criterion and the drawing material considered a perfect plastic material. Rubio et al. [15] published an analytical solution for plate drawing process assuming a perfect plastic material under plane strain condition. Their solution, which has been extended in [16] to consider the material work-hardening, was relatively simple. An upper bound solution to estimate the drawing stress in plate drawing process of materials with no strain-hardening developed by Panteghini [17]. Zhang et al. [18] studied wire drawing through a twin parabolic die by upper bound method assuming perfect plasticity for the rod material.

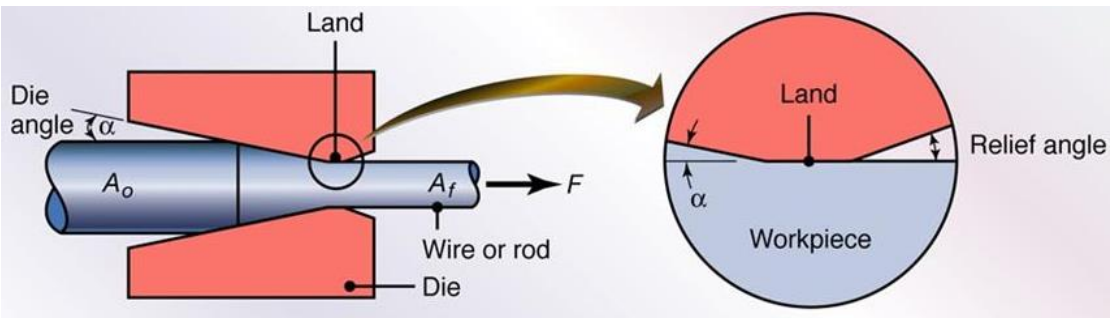


**Figure1** Process variables in rod drawing [1]

According to the literature review, the effect of material properties on the optimum die angle and theoretical studies to determine the effect of material work-hardening behavior on the drawing force and optimum die angle is not studied previously. This paper, studies the effect of the work-hardening characteristics of the rod material on the drawing force and the optimum die angle using upper bound method. The upper bound solution reported by Avitzur [19], based on the assumption of perfect plasticity, has been extended to consider the work-hardening of the material during the rod drawing process. Validity of the proposed approach was demonstrated via conducting experiments and FE simulation using the finite element code DEFORM 2D on the drawing of copper rod material. Other aspect related to the optimization of the process, i.e. the maximum possible reduction in area for different work-hardening exponents, is also investigated.

## 2 Basic equations

### *2.1 Velocity domains*

Figure (1) shows a schematic diagram for the spherical coordinate system $(r,\theta,\varphi)$ and the three velocity domains that are used in the upper bound analysis of rod drawing process through a conical die. Angle $\alpha$ is the angle formed by the die with the axis of the rod, i.e. die angle. The center of the coordinate system is at the converging point of the die surface. The material starts as a round section rod of radius $R_o$ and is drawn into a round section product of radius $R_f$ .

In domain I, the incoming rod is assumed to flow horizontally as a rigid body with a velocity of $v_f$ . In domain III, the drawn rod is assumed to flow horizontally as a un-deformed body with a velocity of $v_f$ . It is assumed that the entire deformation takes place in domain II, that is surrounded by two shear surfaces, $S_1$ and $S_2$ , interface surface as well as the die surface, while in domains I and III the material remains un-deformed. These domains are separated by two shear surfaces $S_1$ and $S_2$ . Surface $S_2$ is the die-material interface, where friction occurs.

The locations of $S_1$ and $S_2$ are at distances $r_o$ and $r_f$ from the origin O, respectively.

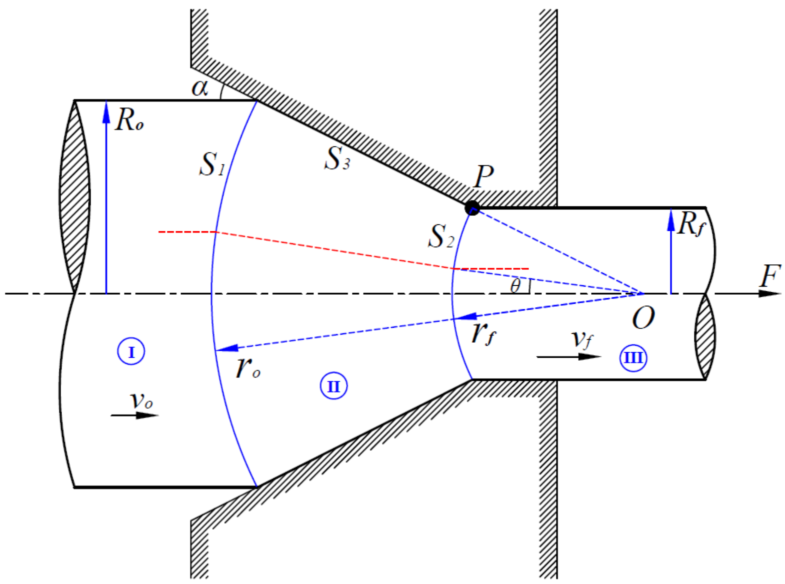


**Figure 2** Schematic diagram of rod drawing process and deformation domains

One classic velocity field, radial flow field, that has been used for the flow through a conical die is the one described as a spherical velocity field [20]. The velocity components in domain II

$$V_r = -v_f \left(\frac{r_f}{r}\right)^2 \cos\theta \,,\, V_\theta = V_\varphi = 0 \tag{1}$$

The strain rates in spherical coordinates are defined as

$$\begin{aligned}
\dot{\varepsilon}_{rr} &= \frac{\partial V_r}{\partial r} \\
\dot{\varepsilon}_{\theta\theta} &= \frac{1}{r}\frac{\partial V_\theta}{\partial \theta} + \frac{V_r}{r} \\
\dot{\varepsilon}_{\varphi\varphi} &= \frac{1}{r\sin\theta}\frac{\partial V_\varphi}{\partial \varphi} + \frac{V_r}{r} + \frac{V_\theta}{r}\cot\theta \\
\dot{\varepsilon}_{r\theta} &= \frac{1}{2}\left(\frac{\partial V_\theta}{\partial r} - \frac{V_\theta}{r} + \frac{1}{r}\frac{\partial V_r}{\partial \theta}\right) \\
\dot{\varepsilon}_{\theta\varphi} &= \frac{1}{2}\left(\frac{1}{r\sin\theta}\frac{\partial V_\theta}{\partial \varphi} + \frac{1}{r}\frac{\partial V_\varphi}{\partial \theta} - \frac{\cot\theta}{r}V_\varphi\right) \\
\dot{\varepsilon}_{\varphi r} &= \frac{1}{2}\left(\frac{\partial V_\varphi}{\partial r} - \frac{V_\varphi}{r} + \frac{1}{r\sin\theta}\frac{\partial V_r}{\partial \varphi}\right)
\end{aligned} \tag{2}$$

Where $\dot{\varepsilon}_{ij}$ (with $i \neq j$ ) is a shear strain rate component.

Based on the velocity field, the strain rate fields for deformation domain II can be obtained by Eq. (2). With the strain rate field and the velocity field, the standard upper bound method can be implemented. This upper bound method involves calculating the internal power of deformation over the deformation zone volume, calculating the shear power losses over the shear surfaces, and the frictional power losses between the material and the die.

### *2.2 The power terms for perfect plastic material*

The general equations to calculate the internal power of deformation $\dot{W}_i$, shear power loss $\dot{W}_S$ and frictional power loss $\dot{W}_f$ for a perfectly plastic material, respectively, are

$$\dot{W}_i = \frac{2\sigma_0}{\sqrt{3}}\int_V \sqrt{\frac{1}{2}\dot{\varepsilon}_{ij}\dot{\varepsilon}_{ij}}\,dV \tag{3}$$

$$\dot{W}_S = \frac{\sigma_0}{\sqrt{3}}\int_S |\Delta V|\,dS \tag{4}$$

$$\dot{W}_f = \frac{m\sigma_0}{\sqrt{3}}\int_{S_f} |\Delta V|\,dS \tag{5}$$

Where $\sigma_0$ is yield stress of perfectly plastic material, $dV$ is a differential volume in the deformation domain and $m$ is friction factor between the die and material.

*2.3 The power terms for work-hardening materials*

The upper bound solution presented in [19] furnishes an estimation of the drawing force during the process under the assumption of a perfect plastic material. Since real metals exhibit work-hardening, some modifications are necessary to adapt the theoretical results based on the assumption of perfectly plastic characteristic to the actual process. A method widely used for this modification is the use of an average flow stress for a work-hardening material.
The average flow stress of the material $\sigma_0$ for the material without work-hardening (perfect plastic material), is given by

$$\sigma_0 = \frac{\int_0^{\bar{\varepsilon}} \bar{\sigma} d\,\bar{\varepsilon}}{\bar{\varepsilon}} \tag{6}$$

When this method is used, the optimum die angle is not affected by the work-hardening characteristics of the material. In order to take into consideration the variation of the optimum die angle due to the work-hardening characteristics, an upper bound method is applied for the radial flow field. The upper bound solution of [19], based on the assumption of perfect plasticity, is extended to consider the work-hardening of the material during the drawing process.

*2.3.1 Equivalent flow stress*

Each particle of the material undergoes different strains in all three domains. So the material has no strain hardening in the domain I, then each particle undergoes a strain due to the discontinuity of velocity at the inlet shear boundary then it undergoes a strain due to deformation in domain II, and respectively the material undergoes a strain due to the discontinuity of velocity in outlet shear boundary and finally it exits from the domain III with no changes in strain level in this domain. According to the position of the particle, the total strain is obtained for the material and it is substituted in power law relationship.

The equivalent strain has been calculated in deformation domain to apply strain hardening effect. The equivalent strain distribution in the rod is calculated by integrating the incremental strain along a stream line which is shown in Figure (1).

The engineering shear strain, $\gamma_{s_1}$ at the inlet shear surface is

$$\gamma_{s_1}(\theta) = \left| \frac{\Delta \mathrm{V}_\theta}{V_r} \right|_{r=r_o} = \frac{v_o \sin\theta}{v_o \cos\theta} = \tan\theta \tag{7}$$

Where $\theta$ is the angular position of a particle on the surface $S_1$.
and this strain is transformed into equivalent strain in the following way:

$$\bar{\varepsilon}_{s_1}(\theta) = \frac{1}{\sqrt{3}} \gamma_{s_1}(\theta) = \frac{1}{\sqrt{3}} \tan\theta \tag{8}$$

The strain imposed in the deformation domain is expressed by

$$\bar{\varepsilon}_d(\theta) = \int_{r_f}^{r_o} d\,\bar{\varepsilon} = \int_{rf}^{ro} \frac{d\,\bar{\varepsilon}}{dt} \frac{dt}{dr} dr = \int_{r_f}^{r_o} \frac{\dot{\bar{\varepsilon}}}{V_r} dr \tag{9}$$

Where $dr$ is the differential length along the radial direction in deformation domain and is the equivalent strain rate and is given by

$$\dot{\bar{\varepsilon}} = \sqrt{\frac{2}{3} \dot{\varepsilon}_{ij} \dot{\varepsilon}_{ij}} = \frac{1}{\sqrt{3}} \sqrt{3\dot{\varepsilon}_{rr} + 4\dot{\varepsilon}_{r\theta}} \tag{10}$$

Placing the Eq. (10) into Eq. (9), then we have

$$\bar{\varepsilon}_d(\theta) = \frac{1}{\sqrt{3}} \int_{r_f}^{r} \frac{\sqrt{3\dot{\varepsilon}_{rr} + 4\dot{\varepsilon}_{r\theta}}}{V_r} dr \tag{11}$$

After integrating, Eq. (11) can be written as

$$\bar{\varepsilon}_d(\theta) = 2\sqrt{1 + \frac{1}{12}\tan^2\theta}\, \ln\frac{r_o}{r_f} \tag{12}$$

The equivalent strain due to the outlet shear surface is

$$\gamma_{s_2}(\theta) = \left| \frac{\Delta V_\theta}{V_r} \right|_{r=r_f} = \frac{v_f \sin\theta}{v_f \cos\theta} = \tan\theta \tag{13}$$

This strain is transformed into the equivalent strain as

$$\bar{\varepsilon}_{s_2}(\theta) = \frac{1}{\sqrt{3}}\gamma_{s_2}(\theta) = \frac{1}{\sqrt{3}}\tan\theta \tag{14}$$

According to the position, the total strain is obtained for the material. The equivalent strain of the particle on the shear surface $S_1$ can be given by

$$\bar{\varepsilon}(\theta) = \bar{\varepsilon}_{s_1}(\theta) \tag{15}$$

In deformation domain II the material is in an intermediate state of deformation, the equivalent strain of the material in the deformation domain, which goes along a streamline, is

$$\bar{\varepsilon}(\theta) = \bar{\varepsilon}_{s_1}(\theta) + \bar{\varepsilon}_d(\theta) \tag{16}$$

The equivalent strain of the points on the shear surface $S_2$, the material is completely deformed and we have

$$\bar{\varepsilon}(\theta) = \bar{\varepsilon}_{s_1}(\theta) + \bar{\varepsilon}_d(\theta) + \bar{\varepsilon}_{s_2}(\theta) \tag{17}$$

After obtaining the total strain and substituting in the hardening relation, the consumption powers can rewrite in order to modify upper bound approach with considering work-hardening of material.

*2.3.2 Power terms*

The internal power in upper bound analysis for a real material, work-hardening material, in the deformation domain is

$$\dot{W}_i = \int_v \bar{\sigma}\dot{\bar{\varepsilon}}\, dV \tag{18}$$

Where $\bar{\sigma}$ is the equivalent flow stress. Internal power of domains I and III are zero and the general equation to calculate the internal power of deformation in domain II is calculated as

$$\dot{W}_i = \frac{2\pi}{\sqrt{3}} \int_{r_f}^{r_o} \int_0^{\alpha} \bar{\sigma}\sqrt{3\dot{\varepsilon}_{rr} + 4\dot{\varepsilon}_{r\theta}}\; (r\sin\theta) r\, d\theta\, dr \tag{19}$$

The general equation for the power losses along a shear surface in an upper bound model is

$$\dot{W}_s = \frac{1}{\sqrt{3}} \int_S \bar{\sigma} \left|\Delta V\right| dS \tag{20}$$

Therefore, knowing the geometry of proposed model (Figure 1) the differential area and the amount of the velocity discontinuity of shear surface $S_1$ can be calculated. The power dissipated on the shear surfaces $S_1$, $S_2$ are determined as

$$\dot{W}_{S_1} = \frac{2\pi}{\sqrt{3}} v_o r_o^{\,2} \int_0^{\alpha} \bar{\sigma} \sin^2 \theta d\theta \tag{21}$$

$$\dot{W}_{S_2} = \frac{2\pi}{\sqrt{3}} v_f r_f^{\,2} \int_0^{\alpha} \bar{\sigma} \sin^2 \theta d\theta \tag{22}$$

The general equation for the frictional power losses along a surface with a constant shear friction factor $m$ is

$$\dot{W}_f = \frac{m}{\sqrt{3}} \int_S \bar{\sigma} \left| \Delta V \right| dS \tag{23}$$

The power dissipated on the frictional surface $S_3$ can be determined as

$$\dot{W}_{f_3} = \pi \frac{m}{\sqrt{3}} v_f r_f^{\,2} \sin 2\alpha \int_{r_f}^{r_o} \bar{\sigma} \frac{dr}{r} \tag{24}$$

*2.4 Drawing force*

Based on the model, the total power can be obtained by summing the internal power and the power dissipated on all frictional and shear surfaces. Then

$$J^* = \dot{W}_i + \dot{W}_{S1} + \dot{W}_{S2} + \dot{W}_f \tag{25}$$

Therefore, the total upper bound solution for drawing force is given by

$$F = \frac{\dot{W}_i + \dot{W}_{s_1} + \dot{W}_{s_2} + \dot{W}_f}{v_f} \tag{26}$$

An integrated MATLAB code was developed to compute the upper bound drawing stress using Eq. (26). For a given process conditions, the program first calculates the velocity components and the strain rate components and then evaluates the upper bound on power. The value of the drawing force obtained in the above-mentioned manner is then minimized with respect to semi-die angle.

## 3 Finite element analysis

The DEFORM-2D, commercial FE code, has been used to simulating the rod drawing process. This kind of tool is very useful because allows to study the influence of some phenomena over the process as, in this case, the work-hardening effect. For this purpose the finite element method is used, simulating the drawing process for different values of work-hardening. Because of the geometry of the problem, only a half of the complete geometry of the process has been modelled.

In the numerical model, the material mechanical behavior has been assumed elasto-plastic. The element type of the mesh is CGAX4R and consists of a 4-node bilinear. These characteristics are appropriate for this element to be used in this type of analysis, where large deformations and contact nonlinearities are assumed. The die is represented by rigid surface elements. The interface between the rod and the die surfaces are represented by interface elements. The typical finite element mesh is presented in Figure (3).

The movement of the rod through the die is simulated by specifying an incremental displacement vector for the first column nodes in the drawing direction until the rod exits from the die as shown in Figure (3).

The flow stress, obtained through curve fitting from the data for electrolytic copper, is approximated by Holloman’s work hardening model as [7]

$$\bar{\sigma}_{cu} = 442(\bar{\varepsilon})^{0.117} \quad \text{MPa} \tag{27}$$

Figure (3) plots the variation of the drawing force during the rod drawing process for both perfect plastic and work-hardening behavior of electrolytic copper rod material. The average flow stress for perfectly plastic material 360 MPa is adopted during the analytical the FE simulation. The shear friction factor was about 0.05 [7]. It is seen that the drawing force initially increases monotonously until the die is completely filled by the drawing billet. Thereafter, the drawing force remains relatively stable.

As shown in this figure, at the early stage of drawing, unsteady state deformation occurs, and the materials have not yet filled up the cavity of the die completely. Thus, the drawing force increases as the drawing process proceeds. After the materials have filled up the cavity of the die completely, the drawing force is constant. From Figure (3), it can be seen that the amount of drawing force employed to carry out the process in the case of work-hardening material is greater than that of perfectly plastic material.

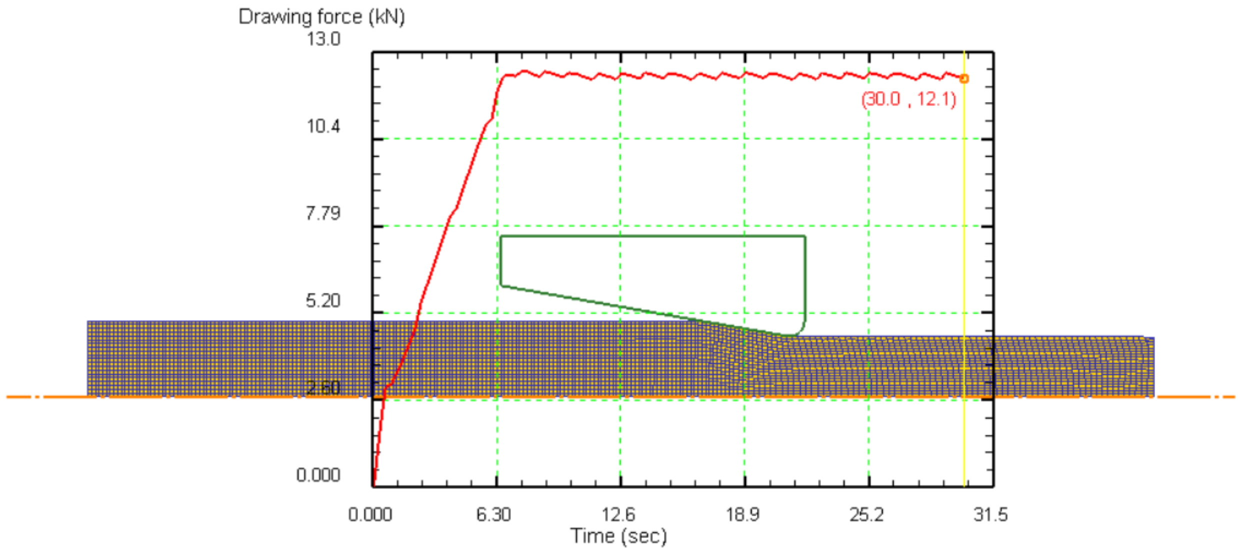


(a) Srain-hardening material

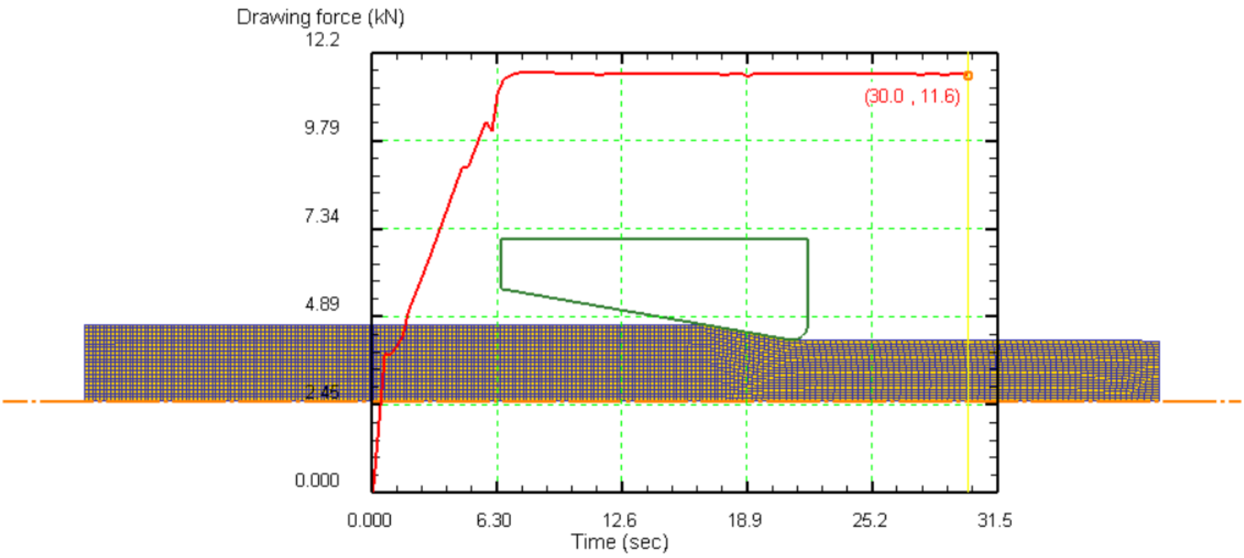


(b) Perfectly plastic material

**Figure 3** Typical distorted meshes and force–time curve; (a) Srain-hardening material (b) Perfectly plastic at the case of $\Phi 10 \rightarrow \Phi 8$ drawing process for friction factor 0.05 and die angle $10^{\circ}$

## 4 Validation of the analytical model

### *4.1 Experiments*

The obvious way to verify the analytical model described in the previous section, would be to compare its results with experimental results covering a suitable range of the parameters of interest. As the working material, copper was chosen. Four different rod geometries have been studied. To obtain various reductions in area, $R_f$ was kept constant and $R_o$ was varied.

The rods were machined to the dimension 150 mm length and they were cleaned with carbon tetrachloride before drawing. The die was conical shape with a semi-angle of 10 °.

The inner surface of the die was mirror polished. The die and its seat in the frame were also cleaned with cotton soaked in the chemical before applying the lubricant for each rod.

A lithium EP3 based grease lubricant was applied manually on the surfaces of the rods and the die just before the draw. A cylindrical block was used to house the die, which was fixed to the holder of the moving cross-head of the testing machine. An experimental setup was manufactured for the rod drawing process and was installed on a 15 ton Universal Testing Machine, which is illustrated in Figure (4) together with a die-set.

Since the experiments were carried out at room temperature and drawing speed was not so high, the process was considered to be free from rate effects. The present study deals with the steady state part of the drawing process. Attention is paid to the drawn length to ensure that it was sufficiently large that steady state conditions were achieved.

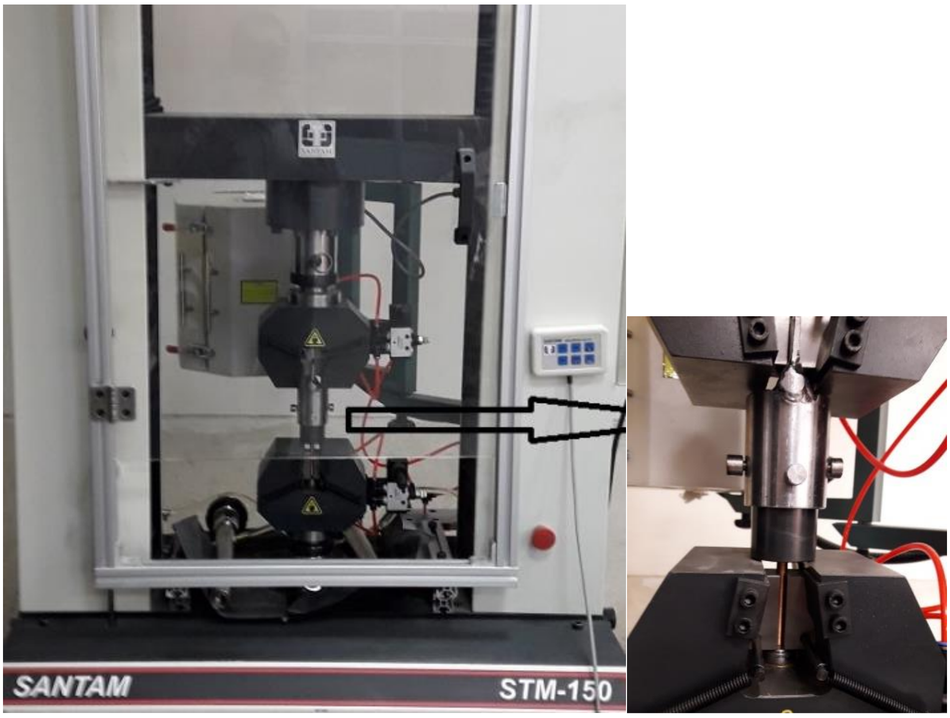


**Figure 4** The 15 kN Universal Testing Machine with a die-set mounted

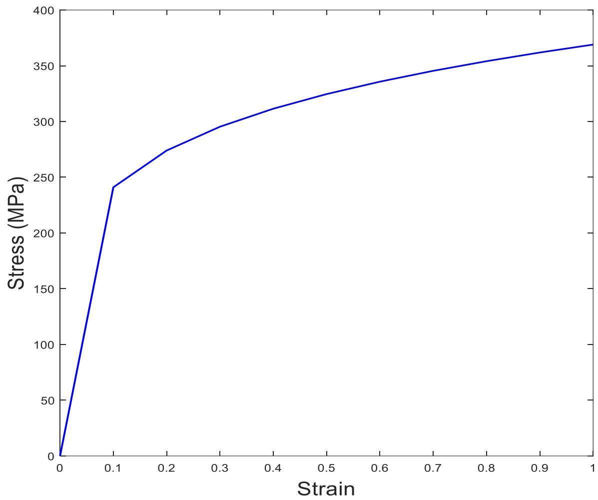


**Figure 5** True stress-strain curve of copper material at room temperature

### *4.2 Determination of mechanical properties*

In order to obtain the stress-strain curve of the material at room temperature, one tensile test piece was also made from copper material. The tensile test was carried out at room temperature at a ram speed of 0.5 mm/min. The true stress-true strain curve obtained for the material, is shown in Figure (5). The flow stresses obtained through curve fitting from the experimental data for copper material is approximated by Holloman's work hardening model as

$$\bar{\sigma}_{cu} = 369.2(\bar{\varepsilon})^{0.185} \text{ MPa} \tag{28}$$

## 5 Results and discussions

The effectiveness of the proposed analytical solution is demonstrated by comparison with both experimental results and the finite element simulation data. In Table (1), the required drawing force obtained by proposed approach, FE and experiments are compared. The results show a good agreement between the upper bound data and the experimental results.

Table (1) also shows that the theoretically predicted drawing forces are higher than FE results and the experimental data due to the nature of upper bound theory. Figure (6) shows the variation of the drawing force with the die angle for perfect plastic material, i.e. Avitzur solution [5], Panteghini solution [7] and work-hardening behavior of electrolytic copper material at the case of $\Phi 10 \to \Phi 8$ drawing process.

**Table 1** Comparison of the calculated, FEM and experimental results of drawing forces

| Drawing case | Measured, kN | Calculated, (kN) | FEM, (kN) |
|---|---|---|---|
| $\Phi 8.5 \to \Phi 8$ | 3.6 | 3.74 | 3.5 |
| $\Phi 9.0 \to \Phi 8$ | 5.4 | 5.53 | 5.5 |
| $\Phi 9.5 \to \Phi 8$ | 7.5 | 7.62 | 7.3 |

| | | | |
|---|---|---|---|
| $\Phi 10. \to \Phi 8$ | 9.3 | 9.45 | 9.2 |

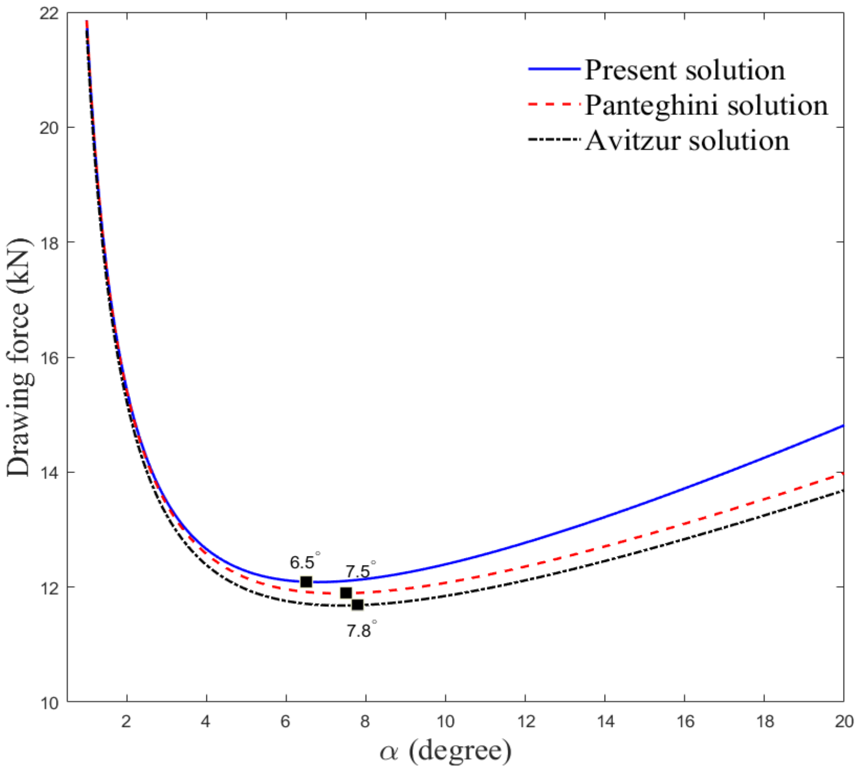


**Figure 6** Variation of drawing force with the die angle at the case of $\Phi 10 \to \Phi 8$ drawing process for copper material, friction factor 0.05

This figure illustrates that the amount of drawing force employed to carry out the process increases as work-hardening of rod materials considers in the solution. It is observed that, there is an optimal die angle, which minimizes the drawing force, and the optimum die angle decreases as work-hardening of rod material considers in the solution. It should be noted that, when perfect plastic material is used, the optimum die angle is the same for different rod materials. Variation of the optimum die angle with work-hardening exponent at the case of $\Phi 10 \to \Phi 8$ drawing process is represented in Figure (7). This figure illustrates that the optimum die angle decreases when the work-hardening exponent increases. The reason for this phenomenon is that increasing the strain-hardenability of a material is equivalent to increasing the sensitivity of its flow stress with respect to the imposed strain. Hence, in such conditions, the rod material would be more susceptible to increase in its flow stress by developing a small strain. Thus, shear power becomes the dominant factor in comparison to frictional power in increasing drawing force, causing the optimum die angle to be reduced to minimize the shear power. This leads to a decrease in the optimum die angle.

Additional computations have shown that work-hardening exponent has an important influence on the magnitude of the drawing force. Figure (8) shows the effect of work-hardening exponent on the drawing force. This figure shows that the drawing force decreases by increasing the strain hardening exponent. The reason for this phenomenon is that increasing the strain-hardenability of a material is equivalent to increasing the sensitivity of its flow stress with respect to the imposed strain. Hence, in such conditions, the flow stress is decreased by increasing of work-hardening exponent value. This leads to a decrease in the drawing force. The most common means of comparing upper bound and FEM results is through drawing force as shown in Figure (8). It is observed that the upper bound results are in good agreement with the finite element results.

These comparisons show that the new analytical model gives good results and could be adopted in the engineering practice as a design procedure to optimize rod drawing processes. As expected, the analytical results by the present method show a good coincidence with the results by the finite element method with a slight overestimation which is due to the nature of the upper bound theory. Comparing the upper bound results and FE results shown in Figure (8), the error is about 5%.

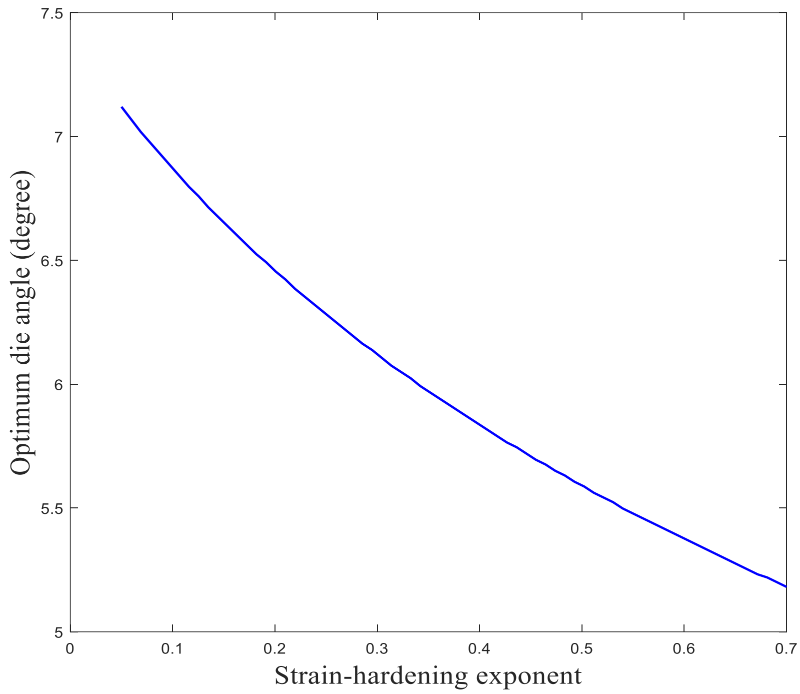


**Figure 7** Variation of the optimum die angle with the strain-hardening exponent at the case of $\Phi 10 \rightarrow \Phi 8$, for friction factor 0.05 and die angle $10^{\circ}$

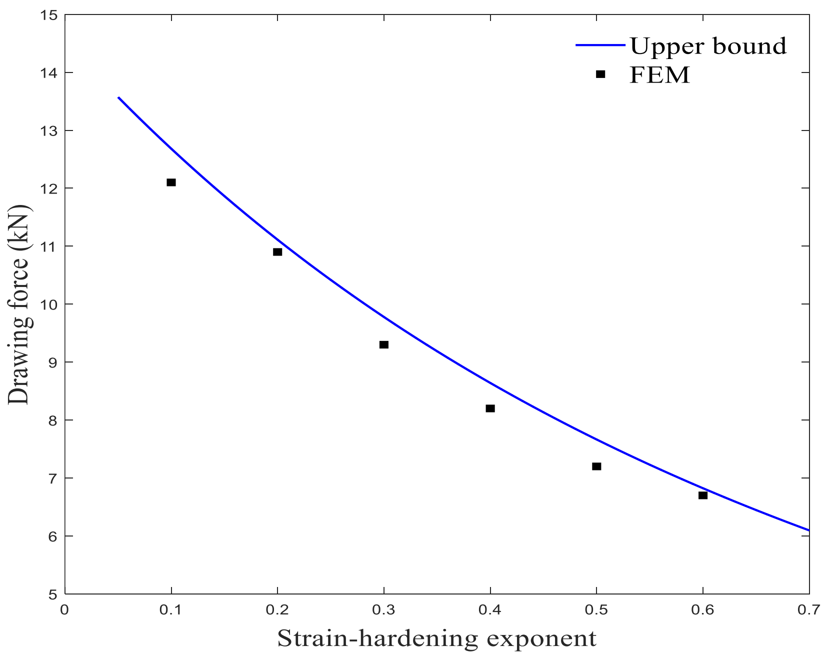


**Figure 8** Variation of the drawing force with the strain-hardening exponent at the case of $\Phi 10 \rightarrow \Phi 8$

drawing process for friction factor 0.05 and die angle $10^{\circ}$

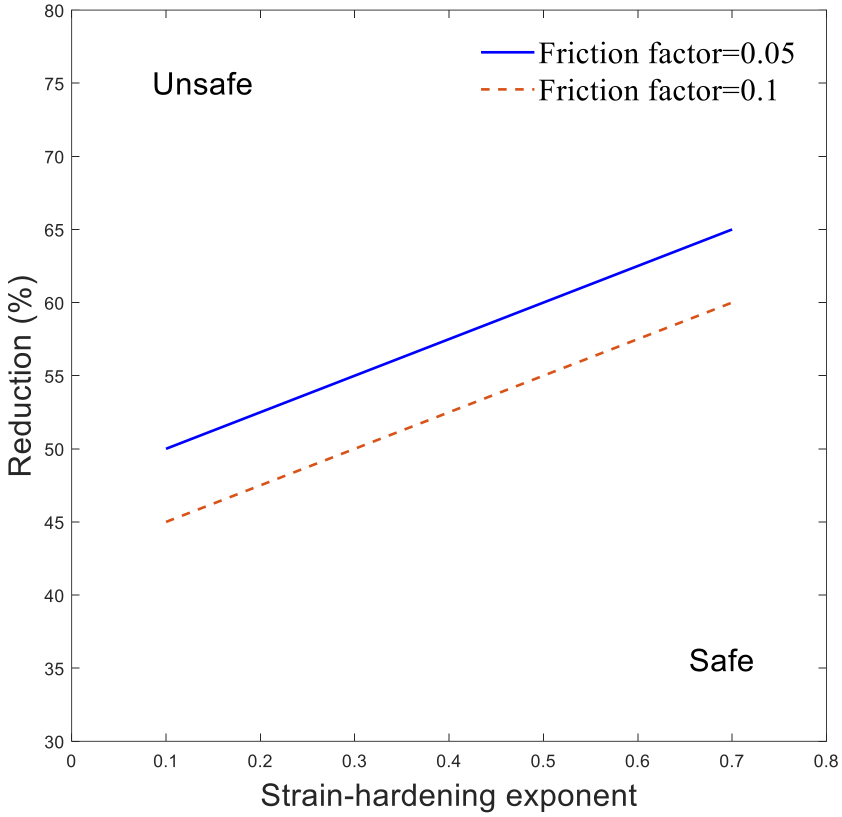


**Figure 9** Variation of the maximum reduction value with the strain-hardening exponent for friction factors 0.05 and 0.1

Of significance for industrial practice is the maximum possible reduction in area. In practice, when a rod is drawn with a reduction in area close to the limiting reduction, the drawn stress is very nearly equal to the flow stress at the exit, so the accuracy of this precept is vitally important. The maximum possible reduction is obtained as a function of the die angle, for several values of the friction factors, equating the drawing stress obtained by the present solution to the flow stress of the material at the exit of the die, i. e. point P in Figure (2).
The maximum value of the reduction in area is calculated for the rod drawing process and the results are plotted in Figure (9). This figure shows the maximum possible reduction for different work-hardening exponent values and two values of the friction factors. The areas under these curves represent possible reductions in area. It can be seen that strain-hardening exponent significantly influences the maximum reduction. Maximum reduction increases when work-hardening exponent increases. From Figure (9), it can be seen that the maximum reduction decreases when friction factor increases. This is due to when friction factor increases, the drawing stress increases.

## 6 Conclusions

In this paper, an analytical solution was proposed for predicting of drawing force in rod drawing process through conical dies based on upper bound analysis. The developed solution is a function of the work-hardening exponent value.

Through the analysis, following conclusions are obtained:
(1) The results afforded by this solution agree with data from experiments and simulations results.
(2) The amount of drawing force employed to carry out the process increases as work-hardening value of rod material considers in the solution.
(3) For a given rod material and process conditions, there is an optimum die angle in which the drawing force is minimized.
(4) The optimum die angle decreases by increasing of work-hardening exponent value.
(5) By increasing the work-hardening exponent, the amount of drawing force decreases.
(6) Maximum permissible reduction increases when work-hardening exponent value increases.

## References


[1] Kalpakjian, S., and Schmid, S.R., "*Manufacturing Engineering and Technology*", Pearson Pearson India, New Delhi, (2018).

[2] Wistreich, J.G., "Investigation of the Mechanics of Wire Drawing", Proceedings of the Institution of Mechanical Engineers, Vol. 169, pp. 654-678, (1955).

[3] Avitzur, B., "Analysis of Wire Drawing and Extrusion through Conical Dies of Small Cone Angle", Journal of Engineering for Industry, Vol. 85, pp. 89–96, (1963).

[4] Avitzur, B., "Analysis of Wire Drawing and Extrusion through Conical Dies of Large Cone Angle", Journal of Engineering for Industry, Vol. 86, pp. 305–316, (1964).

[5] Avitzur, B., "Flow Characteristics through Conical Converging Dies", Journal of Engineering for Industry, Vol. 88, pp. 410–420, (1964).

[6] Critrescru, N., "On the Optimum Die Angle in Fast Wire Drawing", Journal of Mechanical Working Technology, Vol. 3, pp. 275–287, (1980).

[7] Panteghini, A., and Genna, F., "An Engineering Analytical Approach to the Design of Cold Wire Drawing Processes for Strain-hardening Materials", International Journal of Material Forming, Vol. 3, pp. 279–289, (2010).

[8] Chevalier, L., "Prediction of Defects in Metal Forming: Application to Wire Drawing", Journal of Materials Processing Technology, Vol. 32, pp. 145–153, (1992).

[9] Zhao, D. W., Zhao, H. J., and Wang, G. D., "Curvilinear Integral of the Velocity Field of Drawing and Extrusion through Elliptic Die Profile", Transactions of Nonferrous Metals Society of China, Vol. 5, pp. 79–83, (1995).

[10] Zhao, D.W., Wang, G.D., and Zhong, J., "Surface Integral Analysis of Axis-symmetric Drawing through Hyperbolic Die Profile", Applied Sciences, Vol. 14, pp. 224–227 (in Chinese's), (1996).

[11] Rubio, E.M., Camacho, A.M., Sevilla, L., and Sebastian M.A., "Calculation of the Forward Tension in Drawing Processes", Journal of Materials Processing Technology, Vols. 162–163, pp. 551–557, (2005).

[12] Luis, C.J., Leon, J., and Luri, R., "Comparison between Finite Element Method and Analytical Methods for Studying Wire Drawing Processes", Journal of Materials Processing Technology, Vols. 164–165, pp. 1218-1225, (2005).

[13] Chen, D.C., and Huang, J.Y., "Design of Brass Alloy Drawing Process using Taguchi Method", Materials Science and Engineering, Vol. 464, pp. 135–140, (2007).

[14] Gonzalez, H.A., Calvet, J.V., and Bubnovich, V.I., "A New Analytical Solution for Prediction of Drawing Force in the Drawing Process", Journal of Materials Processing Technology, Vol. 198, pp. 93–98, (2008).

[15] Rubio, E.M., Marin, M., Domoingo, R., and Sebastian, M.A., "Analysis of Plate Drawing Processes by the Upper Bound Method using Theoretical Work-hardening Materials", International Journal of Advanced Manufacturing Technology, Vol. 40, pp. 261–269, (2009).

[16] Rubio, E.M., Sebastian, M.A., and Sanz, A., "Mechanical Solutions for Drawing Processes under Plane Strain Conditions by the Upper Bound Method", Journal of Materials Processing Technology, Vols. 143–144, pp. 539–545, (2003).

[17] Panteghini, A., "An Analytical Solution for the Estimation of the Drawing Force in three Dimensional Plate Drawing Processes", International Journal of Mechanical Sciences, Vol. 84, pp. 147–157, (2014).

[18] Zhang, S.H, Chen, X.D., Zhou, J., and Zhao, D.W., "Upper Bound Analysis of Wire Drawing through a Twin Parabolic Die", Meccanica, Vol. 51, pp. 2099–2110, (2016).

[19] Avitzur, B., "*Metal Forming: Processes and Analysis*" New York, McGraw-Hill, (1968).

## Nomenclature

| | |
|---|---|
| $F$ | drawing force |
| $J^*$ | externally supplied power of deformation |
| $m$ | friction factor between rod and die |
| $r, \theta, \phi$ | spherical coordinates |
| $r_f$ | radial position of outlet shear boundary |
| $r_o$ | radial position of inlet shear boundary |
| $R_f$ | final radius of rod |
| $R_o$ | initial radius of rod |
| $S$ | area of frictional surface or shear boundary |
| $V_r, V_\theta, V_\varphi$ | velocity components in spherical coordinate |
| $v_f$ | exit velocity |
| $v_o$ | entrance velocity |
| $\dot{W}_i$ | internal power of deformation |

$\dot{W}_S$ power dissipated on the shear boundaries
$\dot{W}_f$ power dissipated on the frictional surfaces

*Greek symbols*

$\alpha$ die angle
$\Delta V$ amount of velocity discontinuity
$\bar{\varepsilon}$ effective strain
$\dot{\varepsilon}_{rr}, \dot{\varepsilon}_{\theta\theta}, \dot{\varepsilon}_{\phi\phi}$ normal strain rate components in the radial, angular and rotational directions
$\dot{\varepsilon}_{r\theta}, \dot{\varepsilon}_{r\phi}, \dot{\varepsilon}_{\theta\phi}$ shear strain rate components
$\tau$ frictional shear stress
$\bar{\sigma}$ effective stress
$\sigma_0$ mean flow stress of the material